Operation of a Three-Electrode Reactor With Different Electrode Bias Potential Configurations

J. L. Gallego, F. Minotti, and D. Grondona

***Abstract*— The three-electrode plasma reactor for the treatment of polluted gases combines a dielectric-barrier discharge with a remote third electrode, designed to enhance streamer propagation in a relatively large region. In this paper, experimental studies of the electrical magnitudes of the discharge for different electrode bias voltage configurations are presented. Also, the Laplacian electric field distribution in the interelectrode gap is calculated for each configuration. The degradation efficiency of NO in an N_2 atmosphere for the different configurations is also reported. It is found that the discharge is generated only for that electrode bias configuration for which the external electric field promotes the streamer propagation across the electrode gap. Also, for a triggered discharge, the reactor efficiency for the removal of NO changes with the different electrode bias configurations. This result can be explained in terms of the electric field intensity. The configuration with higher external electric field improves the number of streamers propagating in the interelectrode gap so that more reactive species generated in the streamers are effectively entrained in the gas flow to be treated.**

***Index Terms*— Atmospheric-pressure plasmas, discharges (electric), plasma applications.**

I. Introduction

THE treatment of toxic gases emitted to the atmosphere has been a topic of discussion in recent years. To reduce these pollutant emissions different technological methods have been proposed by many research teams around the world. Nonthermal plasma is one of the recognized techniques among them. The energetic electrons of the nonthermal plasma collide with gas molecules generating a wide variety of chemical species that undergo reactions capable of breaking toxic molecules and converting them into nontoxic chemical species.

Different plasma-based systems are usually employed such as those based on pure corona discharges [1], [2], dielectric barrier discharges (DBDs) [3]–[6], and plasma–catalyst hybrid systems [7]–[9]. Since many of these configurations operate at atmospheric pressure, the high electric fields needed to generate the plasma generally require close-lying electrodes, which limits the volume of the active region where the gas to be treated flows.

In previous works [10], the development of a three-electrode discharge with cylindrical geometry, which could be long-time sustained over interelectrode gaps up to 20–25 mm, was presented. The discharge is generated during the positive cycle of the DBD, and besides it has a pulsed nature, being composed of repetitive streamers that are uniformly distributed along the whole DBD electrode length, and that propagate across the interelectrode gap to a remote third electrode. This discharge configuration presents a large plasma volume and a natural, low impedance duct for the gas flow. Based on this discharge configuration, a plasma reactor was developed and its efficiency for the removal of NO in an N_2 atmosphere was studied experimentally and theoretically [11]. The reactor presented a very good performance with energetic efficiencies comparable to the most efficient systems. It was also determined in that work that a good efficiency requires well developed and extended streamers, that fully pervades the gas region. For this reason, in this paper, six configurations of the reactor electrode bias potential are studied and the degradation efficiency of NO in an N_2 atmosphere for the different reactor configurations is reported. Also, the electric field in the interelectrode gap is theoretically evaluated to assess its importance for streamer propagation.

II. Experimental Setup

The experimental setup is schematically shown in Fig. 1. The three-electrode reactor arrangement consists in two disks of adhesive aluminum tape of 50-μm thickness and 19 mm (electrode 1) and 17 mm (electrode 2) respective radius, flush mounted at both sides of a polymethyl methacrylate dielectric disk of 40 mm diameter and 5 mm thick. Electrodes 1 and 2 are the central DBD electrode arrangement.

Manuscript received December 30, 2015; accepted November 14, 2016. Date of publication December 7, 2016; date of current version January 6, 2017. This work was supported in part by the Consejo Nacional de Investigaciones Científicas y Técnicas under Grant PIP GI 11220120100453, and in part by the University of Buenos Aires under Grant UBACYT 20020130100699BA.

J. L. Gallego is with the Facultad de Ciencias Exactas y Naturales, Instituto de Física del Plasma, Consejo Nacional de Investigaciones Científicas y Técnicas, Universidad de Buenos Aires, Buenos Aires 1053, Argentina (e-mail: jlgallego@tinfip.lfp.uba.ar).

F. Minotti is with the Facultad de Ciencias Exactas y Naturales, Instituto de Física del Plasma, Consejo Nacional de Investigaciones Científicas y Técnicas, Universidad de Buenos Aires, Buenos Aires 1053, Argentina, and also with the Departamento de Física, Facultad de Ciencias Exactas y Naturales, Universidad de Buenos Aires, Buenos Aires 1053, Argentina (e-mail: minotti@df.uba.ar).

D. Grondona is with the Facultad de Ciencias Exactas y Naturales, Instituto de Física del Plasma, Consejo Nacional de Investigaciones Científicas y Técnicas, Universidad de Buenos Aires, Buenos Aires 1053, Argentina, and also with the Universidad de Buenos Aires, Buenos Aires 1053, Argentina (e-mail: grondona@df.uba.ar).

Color versions of one or more of the figures in this paper are available online at http://ieeexplore.ieee.org.

Digital Object Identifier 10.1109/TPS.2016.2631408

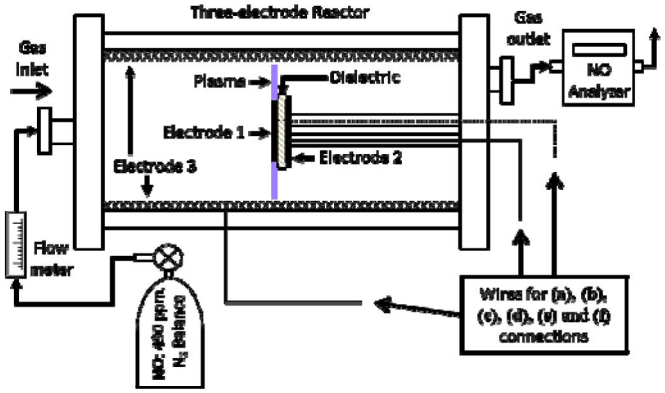

Fig. 1. Experimental setup.

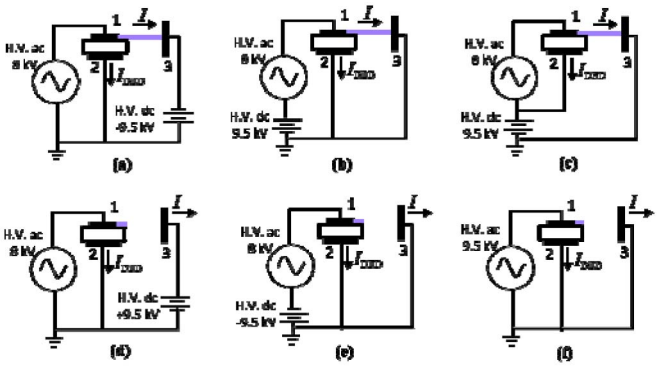

Fig. 2. Different electrode bias configurations, as detailed in the main text.

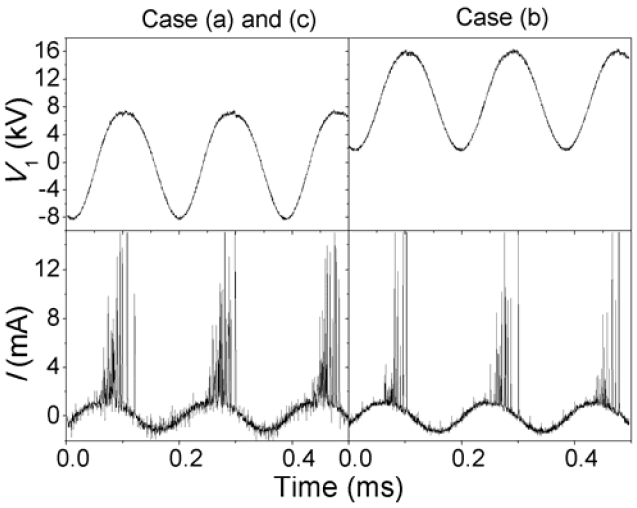

Fig. 3. Typical signals of V_1 and I for configurations (a)–(c).

The disks are connected to the power supply by wires placed inside two insulating tubes (10 mm in diameter) which pass along the electrode system axis. A third coaxial electrode (electrode 3), consisting in a steel mesh is attached to the inner wall of a polymethyl methacrylate dielectric cylindrical tube with 80 mm inner diameter, 240 mm length, and with a wall thickness of 5 mm. This tube contains the central DBD electrode arrangement and the distance between the edges of the DBD electrodes and the electrode 3 is 20 mm. The gas, under pressure, goes through the reactor. Two plates seal the ends of the tube; the gas inlet is placed at one plate and the gas outlet in the other plate.

In this paper, six different configurations of the electrode bias potential were studied. In configuration (a), electrode 1 is connected to the ac power supply, electrode 2 is connected to ground, and electrode 3 to a negative dc power supply. In configuration (b), electrode 1 is connected to the ac power supply connected in series to a positive dc power supply and electrode 2 and electrode 3 are both connected to ground. In configuration (c), electrode 1 is connected to the ac power supply in series to a positive dc power supply, electrode 2 is connected to a positive dc power supply, and electrode 3 is connected to ground. In these three configurations, a surface DBD is generated between electrodes 1 and 2 and a well-developed discharge between electrodes 1 and 3 is also established. We refer to this last discharge as the main discharge. Configurations (d) and (e) are similar to configurations (a) and (b), respectively, but the dc power supply connected is positive. In configuration (f), only electrode 1 is connected to the ac power supply and electrodes 2 and 3 are both grounded. In Fig. 2, a schematic of the six configurations is shown.

The ac power supply consists of a function generator coupled to an audioamplifier (of 700 W) that feeds a high voltage transformer coil. In practice, there was an optimal matching frequency, established by the resonance between the transformer inductance and the capacity of the electrode arrangement. For our circuit geometry, the optimum excitation ac frequency was 5.3 kHz. The ac peak-to-peak voltage was 16 kV and the dc voltage was either −9.5 or 9.5 kV. These voltage intensities are the highest values allowed in the configurations for well-developed discharges without spark generation. The voltage was measured using a high-voltage probe (1000 X/3 pF/100 MΩ). Current measurements were inferred from the voltage drop through a 50 Ω resistance. These electrical signals were registered with a four-channel digitizing oscilloscope with a bandwidth of 60 MHz and 1 GS/s of sampling rate. The operating gas was NO 490 ppm, N_2 balanced. The gas flow Q, measured using a flowmeter, was kept at 1.5 L min^{-1}. The inlet and outlet concentrations of NO were measured by a gas analyzer MaMos 300 with an uncertainty of 1%.

III. Results

The only three configurations in which the main discharge between electrodes 1 and 3 are well generated are configurations (a)–(c). In the other configurations, only a DBD between electrodes 1 and 2 is developed, but no discharge between electrodes 1 and 3 is observed.

In Fig. 3, typical signals of electrode 1 voltage (V_1) and the main current between electrodes 1 and 3 (I) for these configurations are presented. It can be seen in Fig. 3 that the I signal presents more peaks in configurations (a) and (c) than in configuration (b), thus indicating a smaller number of streamers crossing the electrode gap in this configuration.

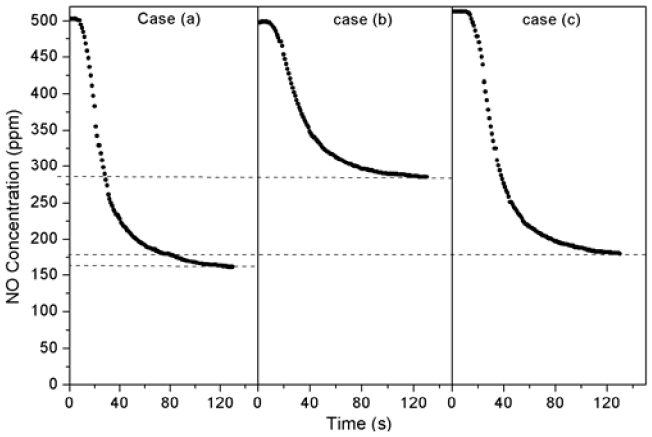

Fig. 4. NO concentration as function of time for the electrode configurations (a)–(c).

TABLE I
REMOVAL EFFICIENCIES FOR ALL WORKING CONFIGURATIONS

Configuration	$\varepsilon_{\text{exp}\%}$
a	67
b	43
c	64

For configuration (a), the onset of the streamers crossing the interelectrode gap occurs at V_1 around 1.4 kV, for configuration (b) at V_1 around 11.1 kV, and for configuration (c) at V_1 around 10.9 kV. The extinction of the streamers crossing the interelectrode gap takes place, approximately, at the maximum value $V_1 = 8$ kV for configuration (a) and $V_1 = 17.5$ kV for configurations (b) and (c).

Fig. 4 shows the time evolution of the NO concentration for configurations (a)–(c), that are the only ones in which a substantial reduction of NO is observed. The initial NO concentration (NO_i) was about 490 ppm, and after the discharge ignition, the NO concentration reached a constant value (NO_f). The final concentration achieved for configuration (a) was $\text{NO}_f = (163 \pm 2)$ ppm, for configuration (b), it was $\text{NO}_f = (286 \pm 2)$ ppm, and for configuration (c), it was $\text{NO}_f = (180 \pm 2)$ ppm.

The removal efficiency of NO ($\varepsilon_{\text{exp}}\%$) was calculated as

$$\varepsilon_{\text{exp}}\% = \frac{\langle \text{NO}_i - \text{NO}_f \rangle}{\text{NO}_i} \times 100. \tag{1}$$

In Table I, the efficiencies for each studied configuration are presented.

IV. INTERELECTRODE LAPLACIAN ELECTRIC FIELD

The Laplacian electric field (E) for all the studied configurations, including those in which the main discharge is not produced, was evaluated using the analytical expression of the potential for a surface charge density inside a cylinder at a fixed zero potential [12]

$$\phi(r,z) = \frac{1}{\pi\varepsilon_0}\int_0^\infty \left\{ \left[\int_0^{a_d} \sigma(r)\, r I_0(kr) dr \right] \times \cos[k(z-z_d)] \left[K_0(kr) - I_0(kr)\frac{K_0(ka)}{I_0(ka)} \right] \right\} dk \tag{2}$$

where, as depicted in Fig. 5, a is the radius of the cylinder, a_d is the radius of the surface charge distribution, located at the axial position z_d, ε_0 is the permittivity of the vacuum, and K_0 and I_0 are the modified Bessel functions of order 0. Expression (2) is valid for any axial coordinate z, and for radial coordinates $a_d \leq r \leq a$. For a single metallic disk of radius a_d lying on the surface of a dielectric of relative permittivity ε_r, the total surface distribution of electric charge, including the charge on the disk plus the polarization charges on the dielectric surface, is given by [13]

$$\sigma(r) = \frac{q_d}{2\pi\varepsilon_r a_d^2 \sqrt{1 - r^2/a_d^2}} \tag{3}$$

where q_d is the electric charge in the disk only. Use of the expression (3) in (2) results in the analytical expression for the potential due to a disk on a dielectric surface, in which the integral in the variable k is to be done numerically. The total potential is obtained as the superposition of the resulting expression for each DBD electrode. This potential, when evaluated at each disk position, allows to relate the disk charges with the disk voltages (which are the actual inputs), and the electric field is finally obtained by numerical spatial derivation.

The radial electric field at $z = 0$ was thus evaluated as

$$E(r, z=0) = -\partial_r \phi(r, z=0). \tag{4}$$

As a check for the correctness of the model of the electric field, we compare the predicted electrode capacitances with the experimentally determined ones.

The theoretical capacitances can be determined considering the case in which the electric field magnitude is insufficient for gas breakdown so that all currents have only a capacitive component. In that case, the relation between the instantaneous electric charge Q_i at the generic electrode i is related to the electrode voltages V_k through the capacitance matrix C_{ik} as

$$Q_i = \sum_{k=1}^{3} C_{ik} V_k. \tag{5}$$

The capacitance matrix is symmetric and also the sum of the elements in each column or row is equal to zero, so that in the particular case of having three electrodes, there are only two independent elements, which can be taken, for instance, to be C_{12} and C_{13}. In this way, assigning alternatively zero charge to electrode 1 or 2 and a given nonzero value to the other electrode, we determine the corresponding electrode voltages and thus C_{12} and C_{13} are obtained from the resulting linear system.

To determine the experimental capacitances, electrode voltage and capacitive currents measurements for configuration (a) with voltage magnitude just below that needed for initiating

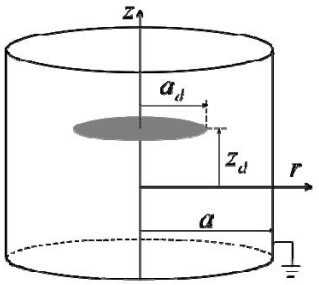

Fig. 5. Schematic showing the electrodes parameters used in the electric field model.

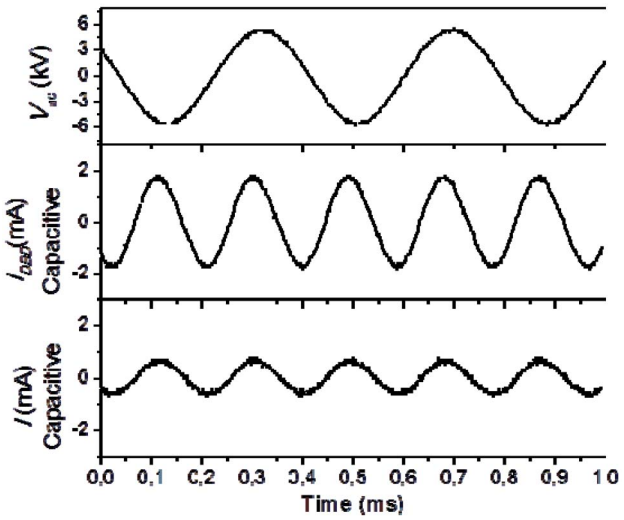

Fig. 6. Electrical measurements of voltage and capacitive currents for configuration (a) for conditions in which there are not discharges.

the discharge were made. Fig. 6 shows the DBD capacitive current (I_{DBD}), and the main capacitive current I for an ac voltage (V_{ac}) of peak-to-peak value equal to 11.4 kV.

Since in the conditions of the experiment $V_1 = V_{\mathrm{ac}}$ while V_2 and V_3 are constant. Also $dQ_2/dt = -I_{\mathrm{DBD}}$, and $dQ_3/dt = -I$, we have from (5) that

$$C_{12} = -\frac{I_{\mathrm{DBD}}}{\dot{V}_{\mathrm{ac}}}, \quad C_{13} = -\frac{I}{\dot{V}_{\mathrm{ac}}}. \tag{6}$$

The capacitances experimental values in (6) were in fact obtained by minimizing the values of

$$\sum\nolimits_n \left(\dot{V}_{\mathrm{ac}}^{(n)} C_{12}^{\mathrm{exp}} + I_{\mathrm{DBD}}^{(n)}\right)^2$$

and

$$\sum\nolimits_n \left(\dot{V}_{\mathrm{ac}}^{(n)} C_{13}^{\mathrm{exp}} + I^{(n)}\right)^2$$

where n indicates a generic measured instantaneous value, so that, finally

$$C_{12}^{\mathrm{exp}} = -\frac{\sum_n I_{\mathrm{DBD}}^{(n)} \dot{V}_{\mathrm{ac}}^{(n)}}{\sum_n \left[\dot{V}_{\mathrm{ac}}^{(n)}\right]^2}, \quad C_{13}^{\mathrm{exp}} = -\frac{\sum_n I^{(n)} \dot{V}_{\mathrm{ac}}^{(n)}}{\sum_n \left[\dot{V}_{\mathrm{ac}}^{(n)}\right]^2}. \tag{7}$$

The obtained experimental and theoretical capacitance values are given in Table II.

TABLE II
EXPERIMENTAL AND THEORETICAL CAPACITANCE VALUES

Capacitance	Experimental (pF)	Theoretical (pF)
C_{12}	-9.6	-9.4
C_{13}	-3.4	-3.5

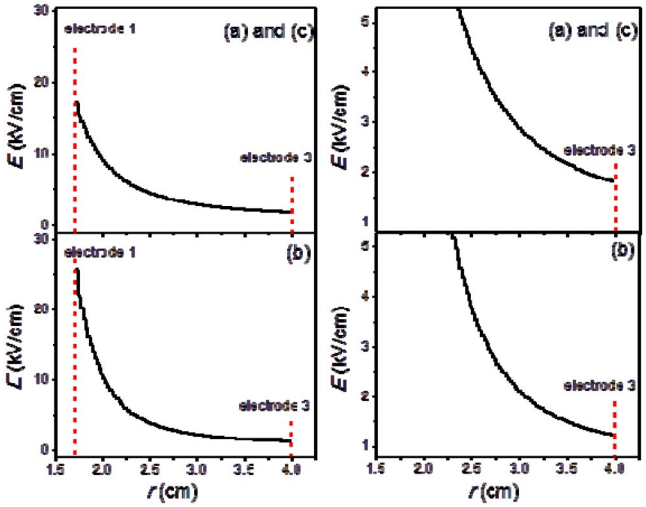

Fig. 7. Radial electric field for (a)–(c) at the onset of DBD for all r positions in the interelectrode gap (left panels) and for radial positions near electrode 3 (right panels).

The good correspondence between experimental and theoretical values of the capacitances gives confidence in the modeled electric field.

Just at the start of the DBD discharge, the electric field is well described by the Laplacian electric field calculated earlier, but once the discharge is ignited, the transported charge accumulates on the dielectric plate and reduces the electric field in the locality of the DBD electrodes, up to the point of interrupting the discharge when the magnitude of V_1 starts decreasing.

In Figs. 7 and 8, the radial electric field at $z = 0$ and at V_1 values at which the onset of the streamers of the DBD takes place, is presented for each configuration.

As can be seen in Fig. 7, the calculated value of the electric field at positions near the electrode 3 ($r = 4$ cm) is higher for configurations (a) and (c), around 1.8 kV/cm, than for configuration (b), around 1.3 kV/cm.

In Fig. 8, it is seen that for the configurations in which the main discharge is not developed, the electric field is either in the opposite direction to that of the streamer propagation, configurations (d) and (e), or, for configuration (f), it is of a substantially smaller magnitude than that in configurations (a)–(c).

V. DISCUSSION

In the studied configurations for which the discharge is well developed, the interelectrode region of the reactor is crossed by long streamers resulting from the propagation of cathode

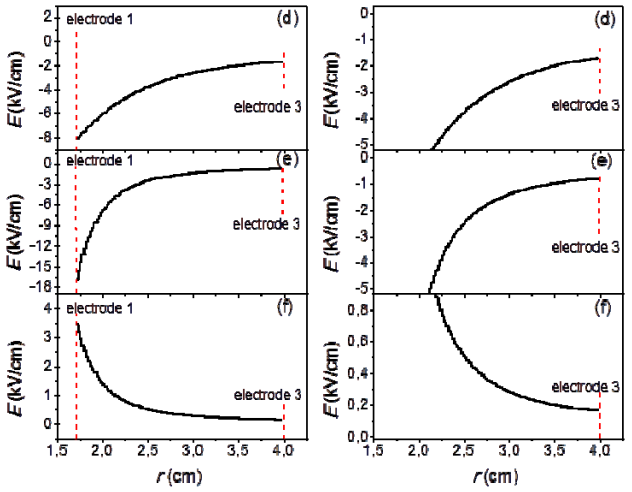

Fig. 8. Radial electric field for configurations (d)–(f) at the onset of DBD for all r positions in the interelectrode gap (left panels) and for radial positions near electrode 3 (right panels).

directed streamers generated between the active electrode of the DBD and a remote third electrode.

It is widely accepted that streamers can propagate stably for long distances only in the presence of an external electric field with a unique minimum electric field value. The minimum electric field for streamer propagation in N_2 at atmospheric pressure is around 1.5 kV/cm [14]. For the configurations for which the main discharge is generated, the external electric field calculated near electrode 3 is around this value, for configuration (b) 1.3 kV/cm, and even higher for configurations (a) and (c), 1.8 kV/cm. The streamer propagation ends after V_1 reaches its maximum, caused by a reduction of the external electric field due to the charge deposited onto the dielectric surface in the DBD electrode system.

In configurations (d)–(f), although the DBD is generated, the main discharge between electrodes 1 and 3 is not produced. For configurations (d) and (e), the external field points in a direction opposite to that of the streamer propagation, and for configuration (f), the external field at almost all radial positions is lower than the minimal external field value required for streamer propagation in N_2.

In those configurations with a well-developed main discharge, the reactor shows a high efficiency in NO removal. The extended interelectrode gap ensures the good pervasion of the streamers into the gas region, and thus the reactive species, generated in the streamer, effectively react with the NO contaminant present in the N_2 working gas. In this paper, the reactor was operated with a DBD dielectric disk thicker (5 mm) than the one employed in the previous work [11] (2 mm) and larger ac voltages could be applied without spark generation; therefore, a larger number of more intensive streamers propagate across the interelectrode gap; thus, the efficiency in NO removal increases. Also, the obtained efficiency in configurations (a) and (c) is about 50% larger than in configuration (b). This result is in total agreement with the experimental observation that a smaller number of streamers cross the electrode gap in configuration (b). These experimental results could be explained in terms of the different external electric fields. For configurations (a) and (c), the streamer propagation to electrode 3 starts with an external electric field at radial positions near electrode 3 slightly higher than that of configuration (b) and this promotes that more streamers propagate across the interelectrode gap.

The development of the main discharge requires two conditions: 1) the presence of a well-developed DBD and 2) an external electric field in the streamer propagation direction that must exceed the minimum electric field value needed for the stable propagation of the streamers across the gap.

References

[1] S. Masuda and H. Nakao, "Control of NOx by positive and negative pulsed corona discharges," *IEEE Trans. Ind. Appl.*, vol. 26, no. 2, pp. 374–383, Mar./Apr. 1990.

[2] K. Shang, Y. Zhuo, and Y. Wu, "Simultaneous removal of SO2/NOx by corona disharge plasma," in *Proc. ICEET*, vol. 3. 2009, pp. 106–109.

[3] A. Mizuno, "Industrial applications of atmospheric non-thermal plasma in environmental remediation," *Plasma Phys. Control. Fusion*, vol. 49, no. 5A, pp. A1–A15, 2007.

[4] A. Khacef and J. M. Cormier, "Pulsed sub-microsecond dielectric barrier discharge treatment of simulated glass manufacturing industry flue gas: Removal of SO_2 and NOx," *J. Phys. D, Appl. Phys.*, vol. 39, no. 6, pp. 1078–1083, 2006.

[5] T. Wang *et al.*, "Effect of reactor structure in DBD for nonthermal plasma processing of NO in N_2 at ambient temperature," *Plasma Chem. Plasma Process.*, vol. 32, no. 6, pp. 1189–1201, 2012.

[6] M. Pacheco *et al.*, "Removal of main exhaust gases of vehicles by a double dielectric barrier discharge," *J. Phys., Conf. Ser.*, vol. 370, no. 1, p. 012023, 2012.

[7] J. Van Durme, J. Dewulf, C. Leys, and H. Van Langenhove, "Combining non-thermal plasma with heterogeneous catalysis in waste gas treatment: A review," *Appl. Catal. B, Environ.*, vol. 78, nos. 3–4, pp. 324–333, Feb. 2008.

[8] M. Dors, J. Mizeraczyk, G. V. Nichipor, and Y. S. Mok, "The role of surface reactions in De-NO_x processes in corona discharge-catalyst (or zeolite) hybrid systems," *J. Adv. Oxidation Technol.*, vol. 8, no. 2, pp. 212–217, 2005.

[9] Q. Yu, H. Wang, T. Liu, L. Xiao, X. Jiang, and X. Zheng, "High-efficiency removal of NO_x using a combined adsorption-discharge plasma catalytic process," *Environ. Sci. Technol.*, vol. 46, no. 4, pp. 2337–2344, 2012.

[10] D. Grondona, P. Allen, and H. Kelly, "Development of a coaxial-stacked trielectrode plasma curtain," *IEEE Trans. Plasma Sci.*, vol. 39, no. 6, pp. 1466–1469, Jun. 2011.

[11] J. L. Gallego, F. Minotti, and D. Grondona, "Experimental and theoretical study of the efficiency of a three-electrode reactor for the removal of NO," *J. Phys. D, Appl. Phys.*, vol. 47, no. 20, p. 205202, 2014.

[12] J. A. Hernandes and A. K. T. Assis, "Electric potential due to an infinite conducting cylinder with internal or external point charge," *J. Electrost.*, vol. 63, no. 12, pp. 1115–1131, 2005.

[13] C. H. Liang, L. Li, and H. Q. Zhai, "Asymptotic closed form for the capacitance of an arbitrarily shaped conducting plate," *IEE Proc. Microw., Antennas Propag.*, vol. 151, no. 3, pp. 217–220, Jun. 2004.

[14] Y. P. Raizer, "Spark and Corona Discharges," in *Gas Discharge Physics*, J. E. Allen, Ed., Oxford, U.K.: Springer, 1991, p. 355.

J. L. Gallego was born in Pereira, Colombia, in 1986. He received his M.S. degree in Physical Engineering from the Universidad Tecnológica de Pereira, Pereira, in 2010. He is currently pursuing the Ph.D. degree with the Institute of Plasma Physics, Consejo Nacional de Ciencias y Tecnología, Faculty of Sciences, Universidad de Buenos Aires, Buenos Aires, Argentina.

His current research interests include nonthermal plasmas.

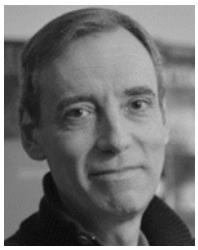

F. Minotti was born in Buenos Aires, Argentina, in 1960. He received the M.S. and Ph.D. degrees from the Universidad de Buenos Aires, Buenos Aires, in 1984 and 1990, respectively.

Since 1993, he is a Researcher with the Consejo Nacional de Investigaciones Científicas y Técnicas (CONICET), Argentina. He is with the Institute of Plasma Physics of CONICET and the Universidad de Buenos Aires, since 1998, where he is currently a Professor.

D. Grondona was born in Buenos Aires, Argentina, in 1964. She received the M.S. and Ph.D. degrees in physics from the Universidad de Buenos Aires, Buenos Aires, in 1989 and 1994, respectively.

Since 1987, she has been with the Institute of Plasma Physics, Consejo Nacional de Ciencias y Tecnología, (CONICET)—Faculty of Sciences, Universidad de Buenos Aires, where she is currently a CONICET Researcher. Her current research interests include nonthermal high-pressure plasmas and RF discharges.